Article

Power Consumption Analysis of a Prototype Lightweight Autonomous Electric Cargo Robot in Agricultural Field Operation Scenarios

Dimitrios Loukatos [ID]**, Vasileios Arapostathis** [ID]**, Christos-Spyridon Karavas *** [ID]**, Konstantinos G. Arvanitis** [ID] **and George Papadakis** [ID]

Department of Natural Resources Management and Agricultural Engineering, Agricultural University of Athens, 11855 Athens, Greece; dlouka@aua.gr (D.L.); varapostathis@aua.gr (V.A.); karvan@aua.gr (K.G.A.); gpap@aua.gr (G.P.)
* Correspondence: ckarav@aua.gr

Abstract: The continuous growth of the urban electric vehicles market and the rapid progress of the electronics industry create positive prospects towards fostering the development of autonomous robotic solutions for covering critical production sectors. Agriculture can be seen as such, as its digital transformation is a promising necessity for protecting the environment, and for tackling the degradation of natural resources and increasing nutritional needs of the population on Earth. Many studies focus on the potential of agricultural robotic vehicles to perform operations of increased intelligence. In parallel, the study of the activity footprint of these vehicles can be the basis for supervising, detecting the malfunctions, scaling up, modeling, or optimizing the related operations. In this regard, this work, employing a prototype lightweight autonomous electric cargo vehicle, outlines a simple and cost-effective mechanism for a detailed robot's power consumption logging. This process is conducted at a fine time granularity, allowing for detailed tracking. The study also discusses the robot's energy performance across various typical agricultural field operation scenarios. In addition, a comparative analysis has been conducted to evaluate the performance of two different types of batteries for powering the robot for all the operation scenarios. Even non-expert users can conduct the field operation experiments, while directions are provided for the potential use of the data being collected. Given the linear relationship between the size and the consumption of electric robotic vehicles, the energy performance of the prototype agricultural cargo robot can serve as a basis for various studies in the area.

Keywords: precision agriculture; autonomous systems; agricultural robots; energy modeling; activity tracking; performance evaluation; embedded systems

1. Introduction

According to the United Nations (UN) organization, the world population is projected to exceed 9.7 billion by 2050 and 10.4 billion by 2100 [1]. Scientists affiliated to the Food and Agriculture Organization (FAO) [2] estimate that there is a need to enhance agricultural productivity, which should be increased by 60% to meet the escalating nutritional demands of the Earth's population. This goal must be pursued despite the ongoing degradation of natural resources, encompassing both a decline in quality and quantity, necessitating simultaneous environmental protection. To address these challenges, the agricultural sector is urged to undergo a transformation, becoming more productive, intelligent, and efficient. The advances in Information and Communication Technologies (ICTs) offer significant opportunities for improvements in agricultural production [3]. This aligns with the principles of Smart Agriculture and Precision Agriculture [4]. Robotics and Autonomous Systems (RAS) technologies could positively contribute to the transformation of the agri-food sector [5–7].

As many field operations are still heavily based on human labor, agricultural production remains susceptible to increased uncertainties, mainly stemming from socio-economic instabilities and pandemics. A notable illustration is the agricultural sector in Europe, where a pronounced shortage of labor has been exacerbated, particularly during the recent COVID-19 pandemic [8,9]. Autonomous farm vehicles are proposed as a solution to challenges in agriculture stemming from a heavy reliance on human labor [10]. Autonomous farm vehicles can achieve comparable outcomes to the conventional ones, at more compact and economic design specifications, as they do not have to carry a human operator, who may weigh more than the machine itself. Robots operate tirelessly, excelling in repetitive tasks at a constant quality level, while humans do not. Furthermore, typical agricultural activities, such as driving tractors on inclined terrains with the risk of overturn [11,12] or engaging in spraying tasks with potentially harmful herbicides and insecticides, pose safety concerns for human operators.

The large size versions of advanced agricultural machines are quite expensive and thus quite unreachable for many farmers with limited financial resources [13]. Conversely, smaller autonomous machines present a viable alternative solution for accomplishing farm tasks, potentially through cooperative operations [14,15], involving fleets of machines with homogeneous or even diverse characteristics [5]. These smaller units also reduce soil erosion and compaction [16] and provide improved maneuverability between the plant rows [17]. Furthermore, if these machines are electric powered, there are environmental advantages, since electric machines do not generate polluting emissions [18]. Considering the skepticism of finding efficient alternative to fossil fuel power sources for modern vehicles [19–21], this study is focused on the electric solutions for small cargo robots. The adoption of electric robotic vehicles can minimize their energy demands by exploiting solar photovoltaic units and batteries for their operation, thus being in line with the recent directions for sustainability and agroecology [22]. In essence, combining agrivoltaics with electric robotic vehicles offers diverse advantages that extend beyond energy demand reduction, fostering a more environmentally friendly and resource-efficient approach to agriculture [23]. This integration, utilizing solar photovoltaics and batteries, not only demonstrates synergy with agrivoltaics but also has broader sustainability implications [24], as it addresses financial constraints faced by farmers by providing a cost-effective and accessible alternative to larger, conventional agricultural machinery [25]. Indeed, a careful selection of components and methods can minimize the footprint of robotic operations in agriculture [26].

On the other hand, too small-sized robots result in very limited usefulness for activities other than crop or soil monitoring [12]. Small-to-medium-sized systems, at least pairing the potential of a farm worker, able to perform several tasks, are seen as the most viable alternative, as they reduce the required financial investment [27] and promote a new production paradigm with significant environmental and social advantages [28]. For the impact of robotics in agriculture to be more easily understood, the agricultural operations should be expressed in terms of actual required workforce (e.g., in work hours per harvested unit of product) for a given level of implemented technology [29]. In this regard, small agricultural robots can be seen as simplified versions of human companions, able to perform useful operations, in the sense of assistive robotics, especially taking under consideration the World Health Organization (WHO) finding [30] that one in seven people experience disability to some extent, and, apparently, many of them are farmers. Consequently, the International Federation of Robotics (IFR) records a growing interest in robots, covering a wide range of activities, as reflected by the recent increase in their sales.

The continuous progress in the electronic industry offers devices of amazing characteristics at affordable prices, fostering the expansion of robots. Many innovative systems are widely available, cost-effective, and sufficiently efficient to support robotic constructions of convincing role and size, combining elements far more economical than those seen a few years ago. A notable example is the Thorvald robotic platform [31] that has evolved to an enterprise offering multipurpose agricultural electric vehicles [32]. Apart from the recent

advancements in the electronics industry enabling vehicles with at least semi-autonomous capabilities at feasible costs, progress in the civilian automotive sector and battery technology further promotes the prospect of electric agricultural vehicles [33,34]. The future trajectory of agricultural robots is anticipated to pivot towards battery-powered systems instead of combustion-based engines [35], contributing significantly to the overall sustainability of agriculture. Hence, the outlook for smart electric robots engaged in agricultural tasks is promising, aligning with the prevailing trend towards sustainable and efficient solutions [36]. The integration of machine learning and artificial intelligence (AI) technologies enhances the capabilities of robotic systems by enabling sophisticated processes such as fruit harvesting [37] and weed detection [38]. The incorporation of machine-learning algorithms allows robotic systems to intelligently identify and harvest fruits with precision, optimizing the efficiency of harvesting operations. Similarly, in weed detection during weeding processes, AI algorithms empower robotic systems to distinguish between crops and weeds, facilitating targeted and precise weed removal without harming the cultivated plants. This integration of machine learning and AI not only signifies the technological strides in agricultural robotics but also underscores the potential for increased automation, accuracy, and sustainability in farming practices [39].

It must be noted that not all agricultural robotic operations are too complex, demanding high-precision equipment. This fact further facilitates the perspectives of the expansion of robotics in agriculture. A notable example is the fruit transportation process, which is much simpler than the fruit collection process itself [18]. Nevertheless, this fact does not make the latter process a less important one, as any potential damage during transportation could have a negative impact on the final fruit quality [40]. This process also remains labor-demanding and harsh to be accomplished by humans, who could be better hired to collect the fruits [18]. Furthermore, recent studies indicate that the optimization of the tray transportation pattern between fruit collection points and trucks, using robot-aided methods, can drastically improve the logistics of the overall harvesting process [41,42].

The forthcoming adoption of electric robotic vehicles in agriculture is directly related to their energy footprint. Therefore, initiatives aimed at modeling, predicting, optimizing, or minimizing their energy usage become of great importance. For instance, the development of accurate models for predicting the energy consumption of agricultural robots can contribute to the reliable estimation of the energy demand during the field operations and result in optimizing the size and location of the smart power grids and the power needed by agrivoltaic installations. Furthermore, the accurate incorporation of the agricultural terrain characteristics (e.g., mud, rocks, vegetation, and inclination) into the behavior models of robots can contribute to optimizing vehicle mission planning in terms of time and energy efficiency.

Despite the aforementioned benefits of investigating the power characteristics of the electric agricultural robots, little progress has been made toward this direction and priority shifting is required. Indeed, numerous studies are directed towards the potential of enhancing the intelligence of robotic vehicles to perform agricultural operations, mainly focusing on (or improving) a single characteristic [43,44]. The examination of literature reviews dedicated to agricultural robotic vehicles [12,27,43–45] reflects the focus of the researchers on improving the intelligence of robots, but it also verifies that only a limited number of works address the energy performance assessment of the robotic platforms [46–48]. The existing scientific landscape indicates that, for the moment, researchers place more emphasis on immediate concerns and challenges, such as functionality and accuracy, rather than delving into the complexities of energy-related aspects, as agricultural robotics, especially in the context of electric vehicles, is still in its nascent stages. In contrast, considerable attention is already paid to the energy efficiency of autonomous vehicles designed for urban environments [49–52], a fact that further highlights the identified research gap and the need for studies providing a deeper investigation of the energy performance of agricultural robotic systems. Therefore, works focused on the energy dynamics, consumption patterns and the overall performance of the agricultural robotic systems are expected to increase

soon. Potential research efforts should provide insights for optimizing the energy consumption, improving the overall efficiency, and ensuring the long-term viability of agricultural robotic systems within the context of evolving agricultural practices and alleviating the environmental considerations.

Willing to contribute toward this direction, this article examines meticulously the energy performance of a typical electric agricultural robotic vehicle throughout characteristic working scenarios under a wide variety of agricultural field terrains. The aim of this work is to provide a deeper understanding of the energy dynamics associated with similar robotic systems, focusing specifically on a smaller model used in practical and typical agricultural applications such as fruit transport. The specific autonomous electric cargo robot [18] exhibits autonomous functionality, thus being able to operate without continuous human intervention. Furthermore, the robot is powered by batteries, signifying its reliance on clean electrical energy for its functioning. This combination of autonomy and battery-powered operation marks the robotic vehicle as an advanced and sustainable solution for common agricultural tasks. The development of a robot having the latter characteristics is important but not sufficient for the objectives being set if not paired with a suitable power behavior monitoring mechanism. For this reason, the present work also describes a simple, flexible, and cost-effective mechanism for a detailed robot's power consumption logging at a fine time granularity, allowing for the detailed tracking and analysis of power usage during the diverse scenarios. In many applications, the battery management system (BMS) operates as an independent unit, without communicating with external systems, and its purpose is to protect the battery without meticulous data gathering or storing [53]. Therefore, an additional strong motivation to implement and utilize the aforementioned mechanism was the absence of experimentation and the deficiencies of commercial counterparts. The former is inadequate while the latter are mostly of closed nature, providing little to no flexibility for customizations of the parameters being measured (e.g., on the data format, the sampling rate, or the point of application) and potentially leading to vendor lock-in phenomena.

In greater detail, the power consumption mechanism being implemented and used combines mostly cost-effective and easy-to-find hardware and software components of a well-documented and open nature that allow for rapid prototype development, efficient measurement collection, and accurate reproducibility. Earlier versions of this mechanism have been used in previous works of our research team [18,54], but not to an extent that fully exploited its potential, while its functionality was further complemented in order to support a flawless measurement collection process. The specific monitoring mechanism exploits many components that already exist on the cargo robot to support its autonomous and adaptive behavior (e.g., microcontrollers, sensors, and storage units). Hence, negligible additional financial cost was necessary for establishing it.

Moreover, in this study, two distinct types of batteries, namely, lead–acid and Li-Po batteries, were tested in each operational scenario. This approach aimed to compare their energy impact on the overall energy efficiency of the robotic system. Notably, Li-Po batteries demonstrated higher efficiencies and significantly lower voltage fluctuations compared to the sealed lead–acid counterparts, resulting in a slightly lower total power consumption. This outcome can be attributed to the reduced weight and internal resistance of Li-Po batteries. The advantages of Li-Po technology include a marked reduction in weight and size, enabling increased energy capacity and autonomy by adding more battery units. This capability positions Li-Po technology as a promising means to optimize energy efficiency and operational endurance in agricultural robotic systems.

Considering the correlation between the performance characteristics of electric machines and their size, particularly for low-speed operations, the power consumption profile will be relevant to larger applications of similar kinds of robotic vehicles. Consequently, the findings of this study offer valuable insights for examining larger electric vehicle configurations and exploring potential cooperative frameworks on a larger scale [50]. Due to the direct relationship between the energy consumption of electric robotic vehicles and their size, specifically their weight [50,55,56], the outcomes of this research can be consid-

ered a reliable pilot case. Therefore, the outcomes can serve as a foundational model for designing larger configurations close to the conventional ones that are currently being used. Furthermore, the measurement approach discussed in this study is highly flexible, based on open and well-documented hardware and software components. The system follows a well-designed and simple architecture, thus making it easily accessible and expandable so as to support further metrics or robotic platforms. Consequently, the proposed setup can function as a flagship for the meticulous analysis of similar robotic activities, describing tools and methods that can be easily adopted by other researchers in the area.

Apart from this introductory section, the rest of this work is organized as follows. Section 2 highlights the underlying mechanism and the methodology behind the measuring process capturing the robot's energy footprint. Section 3 provides analytical performance results for diverse use case scenarios. Section 4 discusses the performance of the robot from the power consumption perspective. Finally, Section 5 contains concluding remarks and plans for the future.

2. Materials and Methods

2.1. Experimental Cargo Robot Details

This section provides the necessary details of the electric cargo robot being used in the experiments as background knowledge for facilitating the energy performance assessment objectives of this work. The latter prototype has a three-wheel chassis equipped with the necessary control and motion components, as depicted in Figure 1, and is capable of both manual and autonomous operation as a harvester companion cargo vehicle. The functionality of this robot is described in detail in [18] and is optimized to pair the potential of a typical farm worker, following a simple, robust, and modular design, based on popular electronic equipment. The basic motion control tasks are performed by an Arduino Uno microcontroller (low-level unit), connected with a more powerful Raspberry Pi credit card-sized computer (high-level unit), for intercepting user commands and/or implementing autonomous behavior characteristics via more composite sensing units, like an accurate global navigation satellite system (GNSS) receiver and a camera.
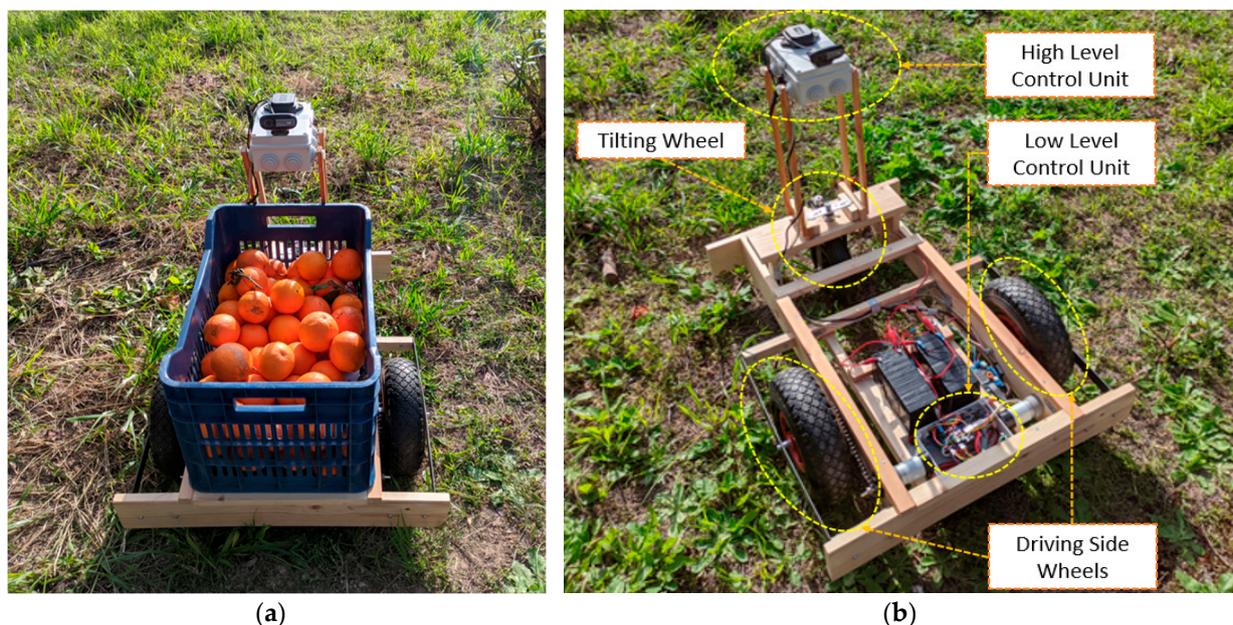

(**a**)   (**b**)

Figure 1. The electric cargo robot used in the experiments. (**a**) Containing a typical cargo of oranges; (**b**) exhibiting its separate functioning modules.

In this regard, the cargo robot can carry a plastic pallet bin full of fruits or vegetables, typically weighting between 10 and 20 kg, between the human collector and the truck, at

the speed of a slow-waking man, i.e., at approximately 0.5 m/s. The robot utilizes two sealed lead–acid battery units of 12 V and 7.2 Ah each, allowing for continuous operations of approximately 3 h. The weight of the robotic vehicle, without cargo and batteries, is around 12 kg, its width is 60 cm, its length is 80 cm, its height (from ground to the top of the bin) is 50 cm, while it also has some of its sensing and controlling components at 70 cm above ground, approximately, for better perception of the surrounding environment when working autonomously. The cargo robot maneuvers utilizing a combination of differential steering, via its driving-side wheels, and tilting, via a third wheel, with both mechanisms to be properly synchronized.

More specifically, the robot can be set up to follow a specific speed and the conformance with this target value is guaranteed by a fine-tuned PID mechanism. It must be noted that it is the steering mechanism that defines the exact target values for the left and the right driving wheel speed, so that the PID works properly. Indeed, as explained in [18], for differential steering, calculations related to the geometry the robot allow for the vehicle to turn at a given speed, following an arc belonging to a circle of a preferred radius.

Let v_o be the desired (and known) speed (i.e., the linear velocity) of the outer wheel, and r_o and r_i be the external and the internal radius of the circles followed by the outer and the inner wheels during this turn, respectively. The distance D between the driving wheels (which is also known) is expressed by the difference between r_o and r_i. As both wheels have the same orbital angular velocity and the linear velocity of the outer wheel remains equal to the one of the vehicle (as a whole) just before steering, the linear velocity of the inner wheel v_i can be easily computed by the D and v_o quantities for a preferred internal turning radius r_i, by the following equation:

$$v_o/r_o = v_i/r_i \text{ or } v_o/(r_i + D) = v_i/r_i \text{ or } v_i = v_o \cdot r_i/(r_i + D), \tag{1}$$

As described in [18], the direction of the non-driving wheel is also adjusted dynamically to conform to the above orbital behavior. More specifically, as the distance between the middle point of its driving wheel distance (D) and the third wheel is also known and equals to L, the angle to turn the third wheel θ is given by the following equation:

$$\theta = \arctan (L/(r_i + D/2)) \tag{2}$$

To transform the above directions into action, during turns the speed of the inner wheel (v_i) is reduced according to Equation (1), while the speed of the outer wheel (v_o) remains unchanged. These values determine the PID mechanism target speed for each driving wheel during turns, while this mechanism follows the same user-provided speed value in straight-line motion cases. The customized PID algorithm being implemented, utilizing pulse feedback from the side motors, adjusts through PWM signals and dedicated motor driving circuits the torque and the speed of each driving-side wheel to anticipate terrain anomalies. In parallel, the vertical axis of the non-driving wheel of the cargo robot is connected to an angle servomotor via a belt drive. Due to this arrangement, during turns, this third wheel synchronizes its angle to conform to the speed modifications of the side wheels according to the calculations provided by Equation (2).

In situ measurements, utilizing both accurate real-time kinematics (RTKs)-assisted GNSS and conventional metering techniques, verified that the robotic vehicle can follow the turning directions with a satisfactory accuracy between 5% and 10% of the r_i quantity, depending on the terrain conditions. In greater detail, the robot should follow specific geometrically defined paths (e.g., straight lines combined with semi-cycles of a specific radius) and its actual path traces, collected in real time, had to be compared against the predetermined ones, thus verifying the turning accuracy of its above-mentioned low-level motion control mechanism. Experiments performed in smooth terrains exhibited differences lower than 5% of the initial radius directions, while in rough terrains, these differences were increased and bounded by 10%.

It is worth noting that not all the functionality potential provided by the specific robotic vehicle was necessary for supporting the experiments described in this article, but its architecture allows for a wide range of modifications to better adapt to the energy footprint measuring requirements required herein. Toward this direction, the main controlling and monitoring functions of interest, as well as the additional arrangements being necessary throughout this study, are further explained in Section 2.2.

2.2. Highlighting the Mechanism for Activity Capturing

The task of extracting reliable results of the performance of the robotic vehicle under a wide set of diverse conditions presupposes the existence of a mechanism allowing for fast and accurate repetitions of the testing scenarios. This mechanism should be easy to use and preferably not require drastic changes in the normal behavior of the robot. These specifications are satisfied by extending the standard controlling functionality, i.e., the software at the remote operator's mobile/tablet device and the sensing elements on the robot. The proposed performance evaluation mechanism establishes a well-defined synergy between a low-level mechanism performing accurate high-granularity measurements (via the arduino microcontroller and pairing sensing equipment), a high-level mechanism for more composite measurements of their storage and management (via the raspberry pi single-board compact computer), and last, but not least, a smart phone device running a suitable application allowing a human to orchestrate the whole process in a simple and comprehensive manner. Details of the overall control and monitoring mechanism of the electric robotic vehicle, as properly updated, are given in Figure 2.
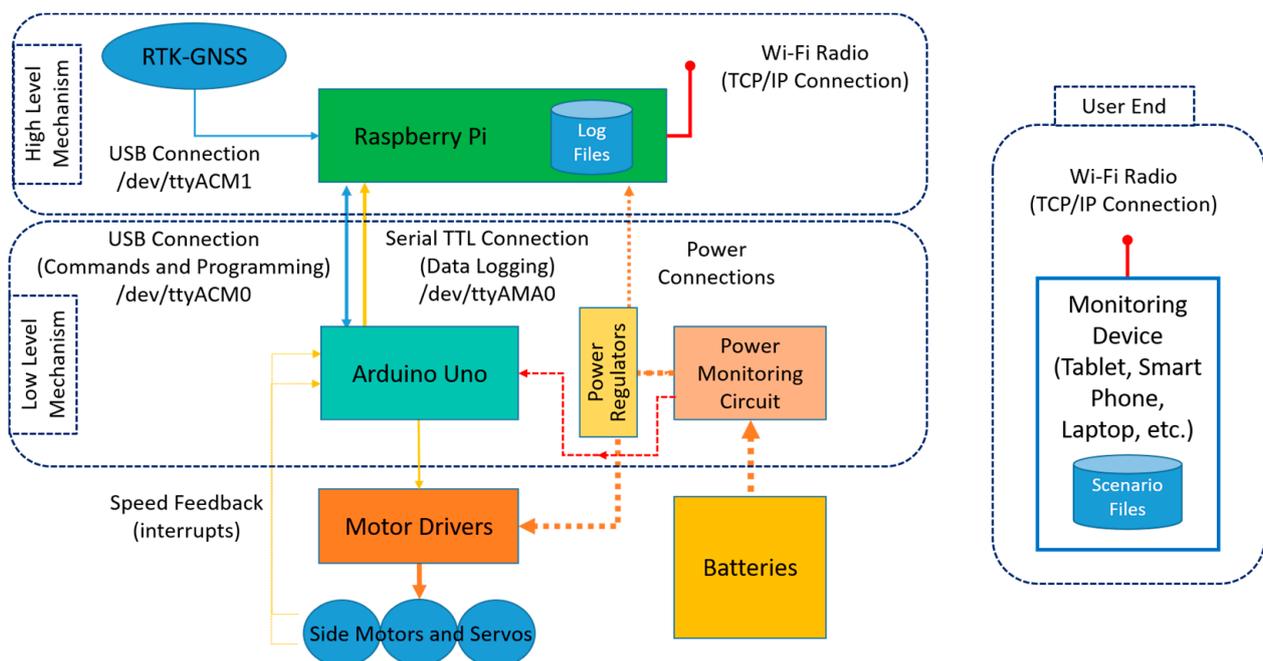

Figure 2. Overview of the main control and monitoring mechanism of the electric robotic vehicle utilized in the experiments.

More specifically, a power metering module, based on the INA219 chip [57], connected with the Arduino Uno via its I2C pins, provided accurate battery voltage and current consumption readings every 0.1 s. Figure 3a depicts the aforementioned chip while Figure 3b illustrates a characteristic code part injected into the arduino microcontroller logic for periodically extracting (and later averaging every 0.1 s) these measurements. While the robot control commands, passed to the low-level microcontroller via the /dev/ttyACM0 interface, the /dev/ttyAMA0 interface of the raspberry pi, accepts the periodic information flow containing the status of the vehicle, Python scripts, like the one presented in Figure 3c,

facilitate the handling of this microcontroller-originated logging information on the Raspberry Pi. In parallel, an assistive RTK-GNSS system provided accurate position verification during the experimental process, utilizing two ZED-F9P modules [58], one installed on the robot (rover) and one fixed (base station), providing RTCM correction messages via two pairing radio modems connected with the corresponding ZED-F9P units via their serial interfaces.
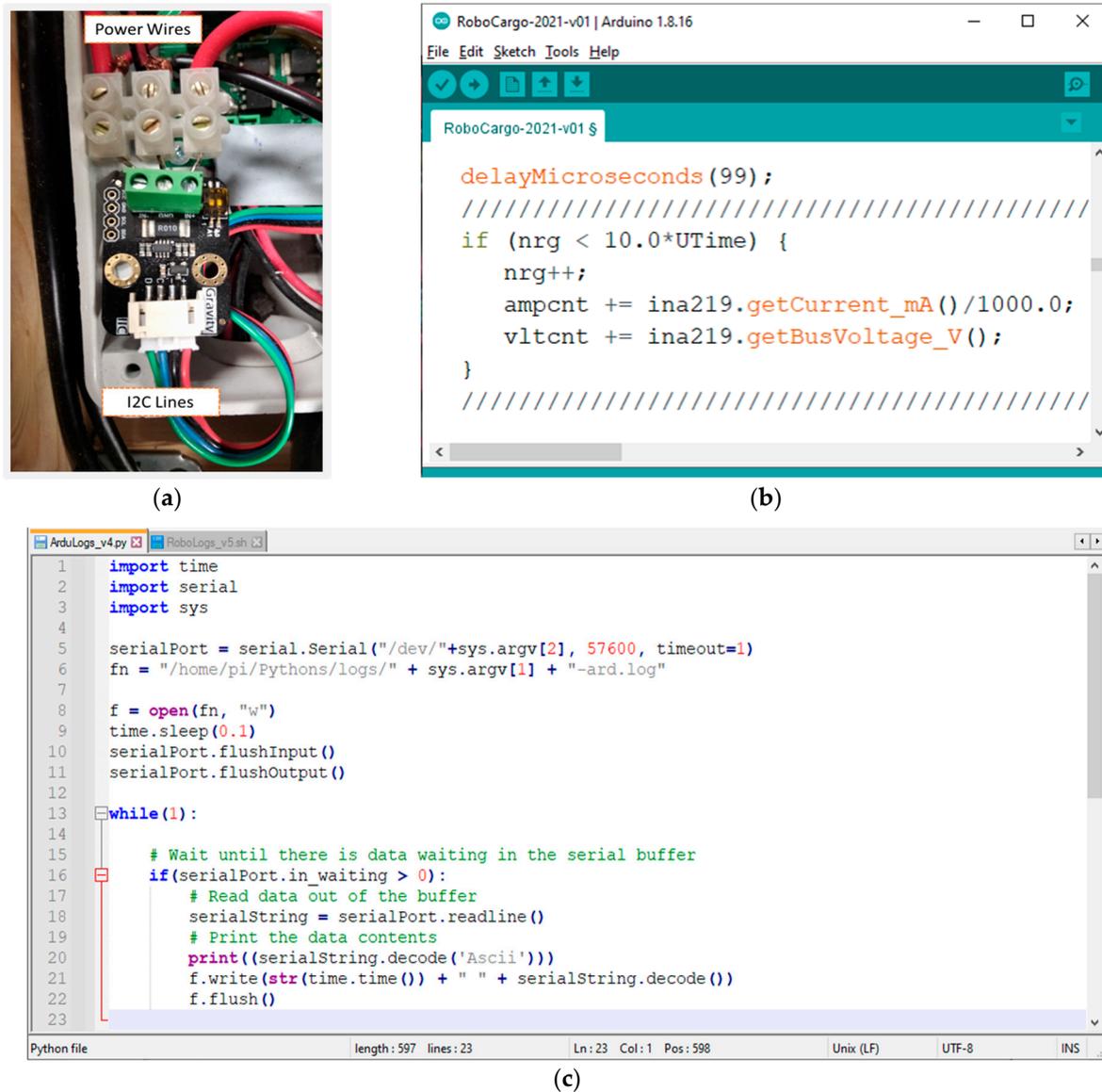

(a)

(b)

(c)

Figure 3. (**a**) The INA219 measuring circuit as incorporated into the robot; (**b**) a characteristic microcontroller code part for extracting current and voltage measurements; (**c**) a Python script for handling the microcontroller-originated logging information.

The electric robotic vehicle behavior can be easily controlled and inspected via an in-purpose implemented mobile application using the MIT App Inventor environment [59]. This application was further modified to support the selection and execution of user-defined scenario files. Algorithmically speaking, an additional countdown timer is used to wait for the necessary interval between the consecutive commands that are sent to the robot. The whole scenario has the form of a text file, each line of which corresponds to a specific action of the robotic electric vehicle. The first parameter in each line denotes the time moment that the specific command must be invoked. The granularity of a second is considered enough

for the scenarios being planned. Each line command is translated into a TCP/IP request to the listening entity of the robot, i.e., the Raspberry Pi. The option to cancel a scenario under execution is also provided to save time and prevent excessive electromechanical stress and energy losses in case of failures/miscalculations. Prior to prompting for scenario execution, the user should activate the file logging operation and deactivate it after scenario completion. An instance of the corresponding code blocks, the application's interface, and an indicative scenario file are depicted in Figure 4a, Figure 4b, and Figure 4c, respectively.
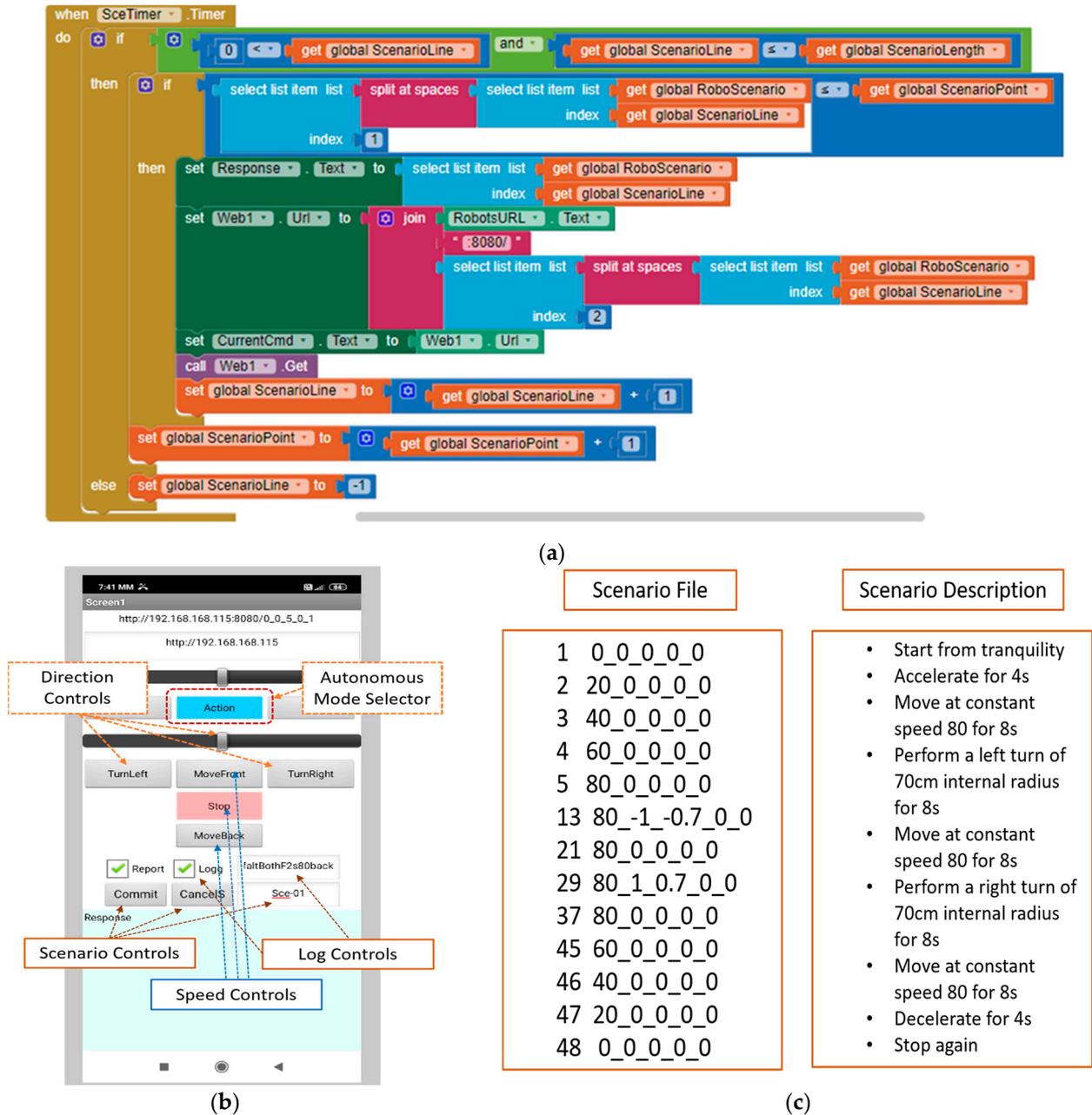

(**a**)

(**b**)

Scenario File	Scenario Description
1 0_0_0_0_0 2 20_0_0_0_0 3 40_0_0_0_0 4 60_0_0_0_0 5 80_0_0_0_0 13 80_-1_-0.7_0_0 21 80_0_0_0_0 29 80_1_0.7_0_0 37 80_0_0_0_0 45 60_0_0_0_0 46 40_0_0_0_0 47 20_0_0_0_0 48 0_0_0_0_0	• Start from tranquility • Accelerate for 4s • Move at constant speed 80 for 8s • Perform a left turn of 70cm internal radius for 8s • Move at constant speed 80 for 8s • Perform a right turn of 70cm internal radius for 8s • Move at constant speed 80 for 8s • Decelerate for 4s • Stop again

(**c**)

Figure 4. (**a**) An instance of the corresponding code blocks; (**b**) the application's interface; (**c**) indicative scenario file.

The monitoring readings of interest were gathered at the flash memory of the Raspberry Pi unit for further processing, while short-period averages were posted to the user's smart phone for fast inspection. In greater detail, the detailed readings were stored into .log and .gps files in the Raspberry Pi micro-SD card. A typical log file is depicted in Figure 5,

containing as record fields the system timestamp, the requested speed for the robot, the corresponding turning radius, an indication if it should turn to the right or to the left or to move straight, the target and actual speed for each of its driving wheels, and, finally, the battery voltage and the overall current consumption. All of this information is recorded at a frequency of 10 times per second.
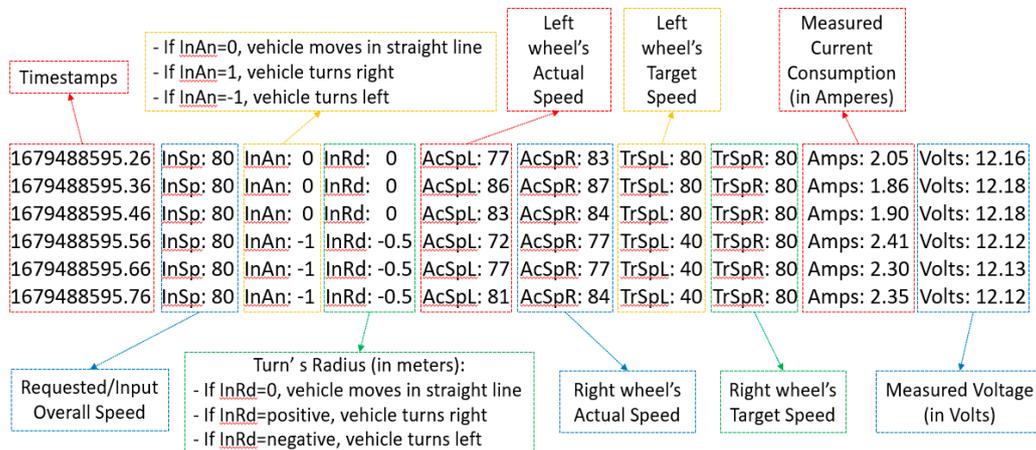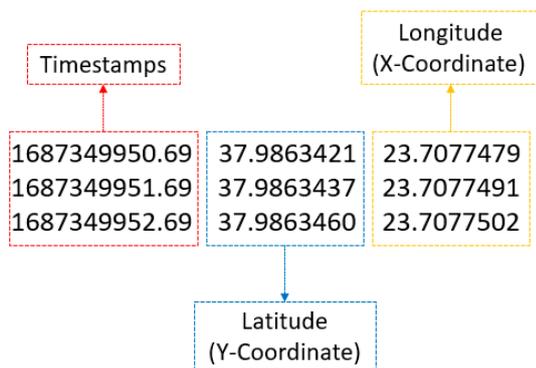

Figure 5. A typical log file of the electric robot.

Similarly, a typical .gps file record, as can be seen in Figure 6a, contains the system timestamp and the latitude and longitude information of the robot at any given time. The .gps file is appended with new data once per second. The presence of an RTK-GNSS provides high positioning accuracy with a divergence lower than 2 cm, and thus, for assistive purposes, the potential activity scenarios of the robot can be better verified and documented rather than only relying on in situ visual inspection by a human observer. Indeed, the GNSS data being recorded can be later processed, resulting in traces that visualize the motion of the robot using the QGIS software (version 3.32) [60], as can be seen in Figure 6b, where a scenario case is depicted according to which the electric robotic vehicle was moving on asphalt terrain from the bottom left to the upper right.

(**a**)   (**b**)

Figure 6. Position and tracing of the electric robot: (**a**) details of a typical .gps file instance; (**b**) the visualization of its movement in the QGIS environment.

Hence, the whole mechanism guarantees that a specific time sequence will be followed by the robot throughout the diverse terrain tests, which is quite difficult to be carried out

by detailed manual commands given by humans, which are not famous for their ability to perform repetitive tasks at a constant manner.

2.3. Activity Scenario Description

Typical robotic field operation scenarios are selected in order to better reveal and capture the dynamics of the vehicles. These scenarios include mainly straight-line circuits at a constant speed on horizontal and inclined surfaces, and U-turns. The same robotic vehicle field operation scenario is repeated under diverse terrain, cargo, and speed conditions. Finally, the standard sealed lead–acid batteries are replaced with Li-Po batteries of equivalent capacity and voltage in order to study the impact of this power source change on the energy footprint of the robotic vehicle.

In greater detail, the discussed field operation scenarios include the following:

1. The "ramp" scenario: a straight-line circuit from idle with an increase in speed of 10% (i.e., of the maximum speed) every 15 s until the robot reaches its maximum speed;
2. The "steps" scenario: a straight-line movement with two levels of speed, 40% and 80% of the robot' s maximum speed, namely, 0.3 m/s and 0.6 m/s, respectively;
3. The "U-turn" scenario: where the robot moves constantly with 80% of its maximum speed, namely, 0.6 m/s, and performs two U-turns, forming an "S" symbol with its movement;
4. The "inclined" scenario: a straight-line circuit at a constant speed, 40% and 80% of the robot's maximum speed, i.e., 0.3 m/s and 0.6 m/s, respectively, initially on flat and then on 10% inclined asphalt terrain.

The "ramp", "steps", and "U-turn" scenarios have each been conducted in three different kinds of terrains, including asphalt, grass, and rough field. Furthermore, all the above scenarios have been conducted with a typical cargo that weighed 15 kg or without cargo. In all of these scenarios, the power consumption was measured in order to highlight the differences between the various cases. Additionally, for the scenarios (or scenario segments) with a constant target speed, such as the "steps" scenarios, the average power, in Watts, was calculated, as it was consumed during the robot's motion throughout each of these scenarios (or segments).

Apart from the above testing action classification, the standard pair of sealed lead–acid 12 V batteries of 7.2 Ah each powering the robot were replaced with 3-cell Li-Po batteries of 11.1 V and 4 Ah each, and the most indicative experiments were repeated. This battery type alteration was an equivalent voltage and capacity arrangement, as a sealed lead–acid batteries are recommended to be discharged up to 50% of their total capacity, i.e., each of the ones being used to provide up to 3.6 Ah to the robot, while a Li-Po battery is typically discharged up to 80% of its total capacity, which is translated to 3.6 Ah available for the robot as well.

As with the diverse terrain scenarios, for comparing the two battery types, i.e., the sealed lead–acid and the Li-Po ones, the power consumption and the battery voltage were measured to analyze their energy impact. Under constant target speed conditions, the average power and voltage were calculated to study the efficiency of the two battery types. Furthermore, the voltage deviation was calculated to deduce which battery type exhibited more voltage fluctuations, because the voltage fluctuations typically reduce the battery life expectancy and may have a negative impact on the system electronics operation.

3. Experimental Deployment and Results Evaluation

3.1. Applying the Testing Scenarios

In accordance with the testing scenario specifications explained in Section 2.3, field experiments were performed on asphalt, grass, rough, and inclined terrains, with and without cargo, as depicted in Figure 7. Furthermore, the performance of the electric robotic vehicle running on Li-Po batteries instead of sealed lead–acid ones was also evaluated, as depicted in Figure 8. In all cases, the corresponding activity was coordinated via the

in-purpose implemented mobile application, while the resulting log files were collected from the Raspberry Pi memory card for further post-processing.
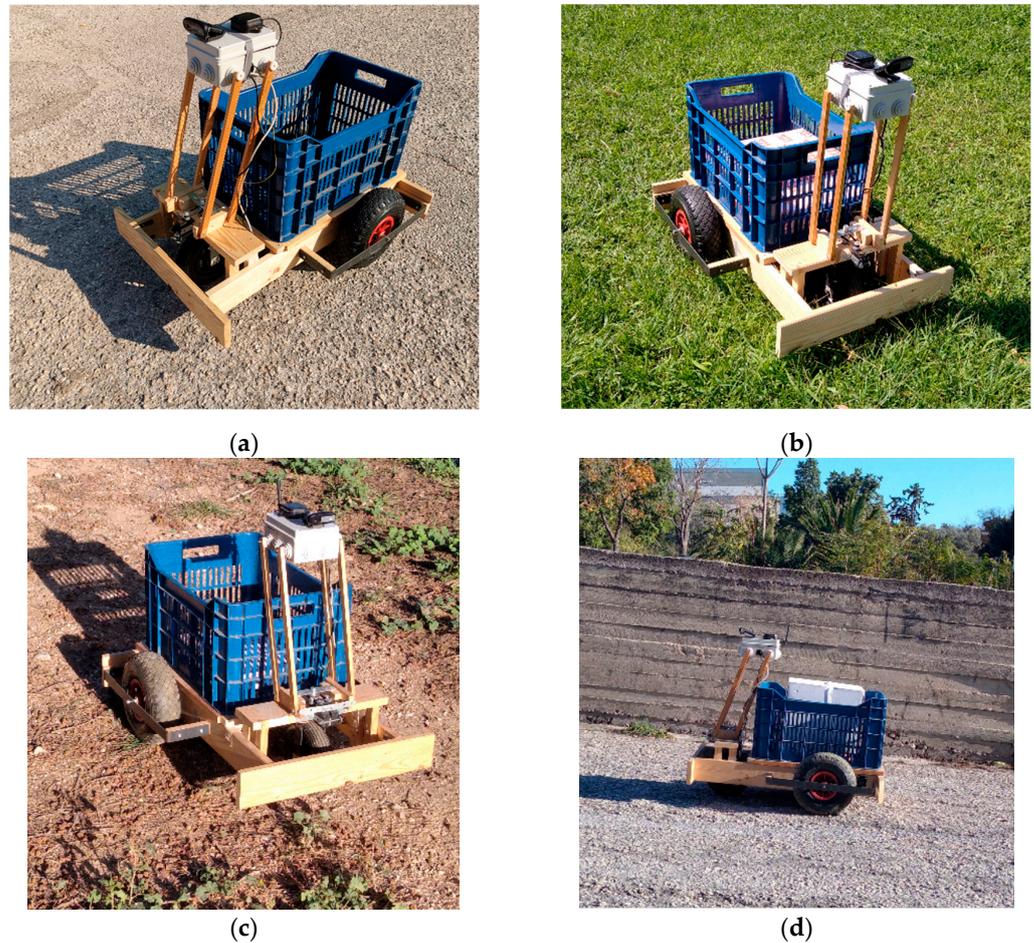

Figure 7. Diverse scenario settings on the following: (**a**) asphalt; (**b**) grass; (**c**) rough soil; (**d**) inclined terrains.
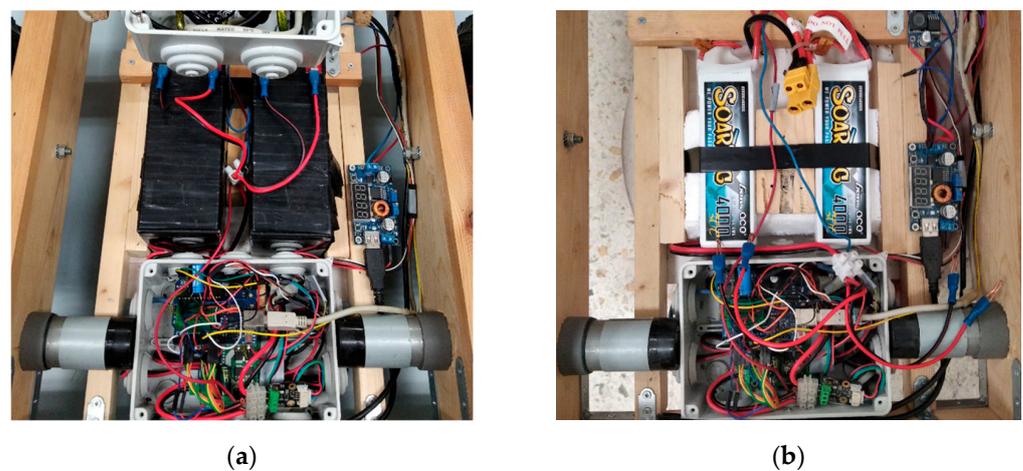

Figure 8. Different power source settings, including: (**a**) sealed lead–acid batteries; (**b**) Li-Po batteries.

3.2. Results Visualization and Analysis

During the experiments of the described scenarios, data were gathered in the corresponding .log files. These data were further post-processed and analyzed to study the

energy footprint of the electric robotic vehicle during the various scenarios. For all scenarios, the voltage and current being measured were used to calculate the instantaneous power consumption in Watts, thus resulting in time diagrams with the X-axis in seconds. Additionally, for the better assessment of the differences between sealed lead–acid and Li-Po batteries, voltage diagrams were created, highlighting the behavior of each battery type.

Finally, for a more fluent performance comparison, statistical average values of power consumption were calculated during the scenarios, or sections of them, characterized by constant target speed levels. Similarly, voltage deviation was calculated to compare the voltage fluctuation intensity that was experienced during the electric robotic vehicle's motion for each battery type, i.e., the sealed lead–acid and Li-Po ones.

In this regard, Figure 9 presents the comparative power consumption diagram with (indicated by red color) and without cargo (indicated by blue color) for the ramp scenario, using lead–acid batteries, in asphalt terrain (a), grass terrain (b), and rough field terrain (c). As depicted in Figure 9, scenarios involving cargo exhibit higher power consumption compared to those without it, as the added weight imposes a greater load on the batteries.
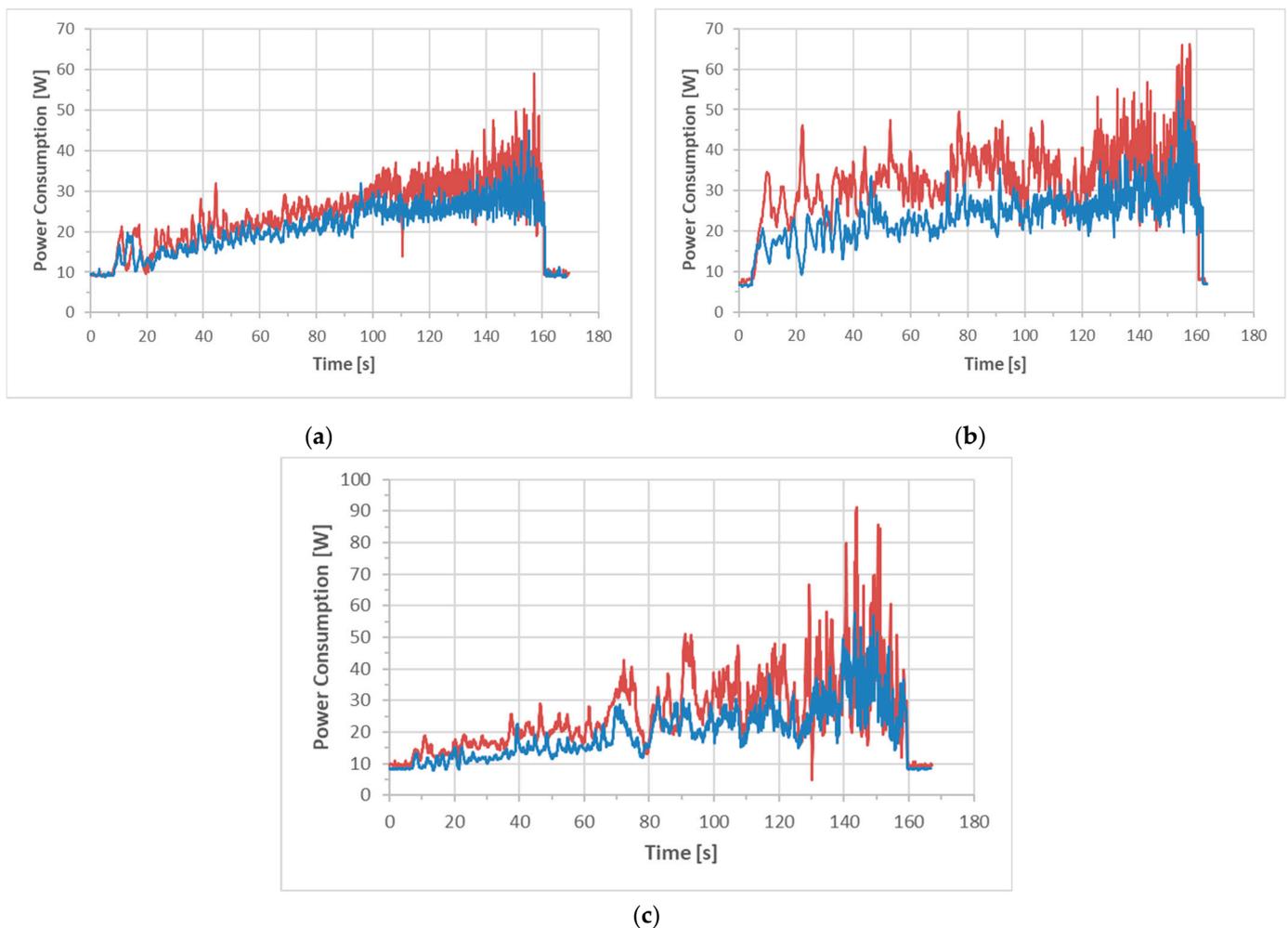

(**a**)

(**b**)

(**c**)

Figure 9. Power consumption with cargo (red color) and without cargo (blue color) for the "ramp" scenario in the following: (**a**) asphalt terrain; (**b**) grass terrain; (**c**) rough field terrain.

Figure 10 presents the comparative instantaneous power consumption variation with (red color) and without (blue color) cargo for the step scenarios using lead–acid batteries on asphalt terrain (a), on grass terrain (b), and on rough field terrain (c). Steps scenarios are ideal for capturing the energy behavior of the robot at constant conditions for different speed settings, i.e., at 0.3 m/s and 0.6 m/s. As it can be inferred via the inspection of the

corresponding to the above scenarios average data provided in Tables 1–3, the average power calculated for the cases with cargo loaded on the robotic vehicle is higher than without cargo, in both speeds, as expected.
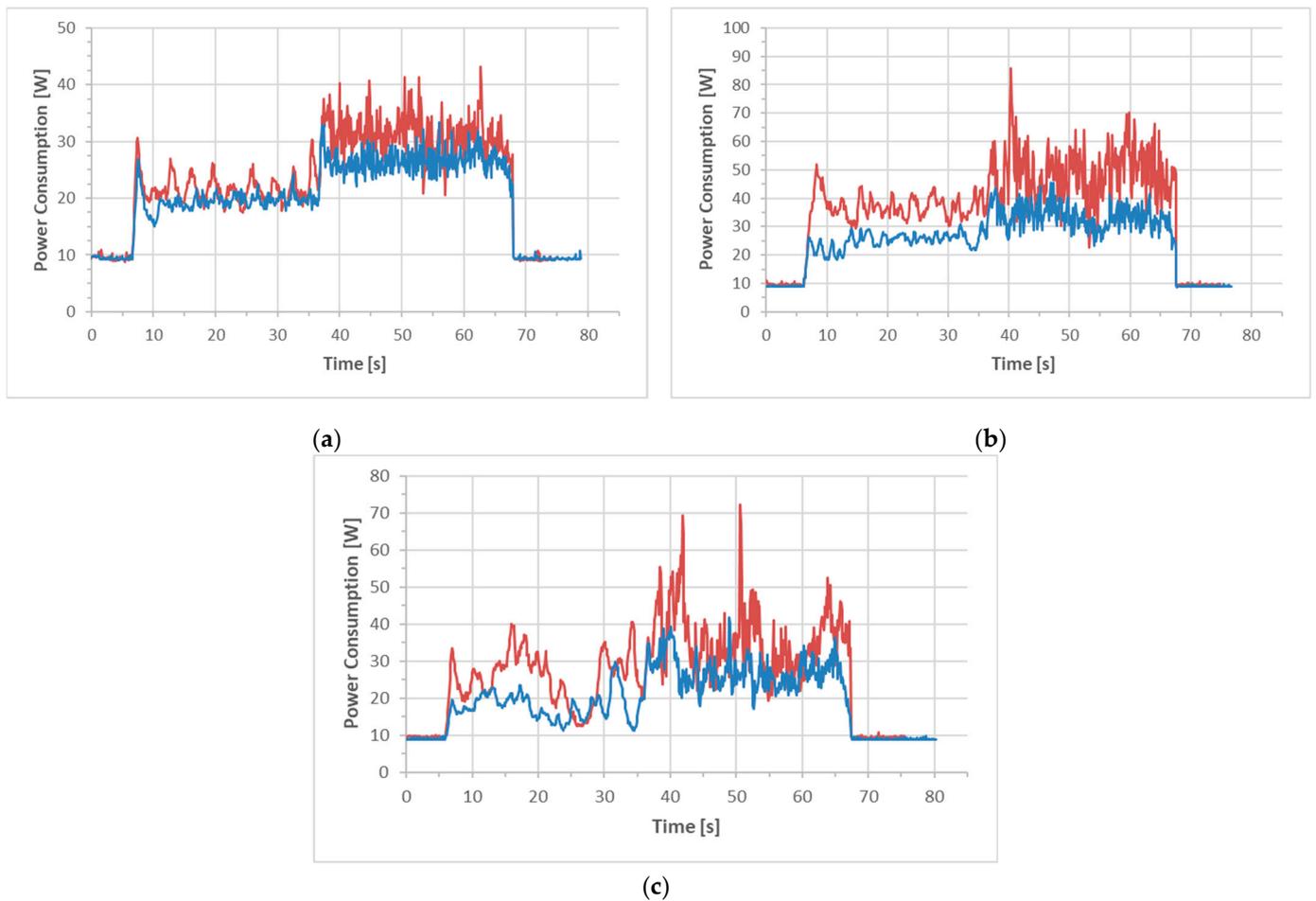

(**a**)

(**b**)

(**c**)

Figure 10. Power consumption with (red color) and without (blue color) cargo for the steps scenarios, using lead–acid batteries, on the following: (**a**) asphalt terrain; (**b**) grass terrain; (**c**) rough field terrain.

Table 1. Power consumption statistics about the steps in the asphalt terrain scenario using lead–acid batteries.

Steps in Asphalt Terrain	P Average at 40% Speed	P Average at 80% Speed
Without Cargo	19.4 W	26.6 W
With Cargo	21.6 W	31.1 W

Table 2. Power consumption statistics about the steps in the grass terrain scenario.

Steps in Grass Terrain	P Average at 40% Speed	P Average at 80% Speed
Without Cargo	22.9 W	31.9 W
With Cargo	36.7 W	49.0 W

Table 3. Power consumption statistics about the steps in the rough field terrain scenario.

Steps in Rough Field Terrain	P Average at 40% Speed	P Average at 80% Speed
Without Cargo	20.8 W	27.2 W
With Cargo	25.5 W	35.5 W

Figure 11 presents the power consumption for the U-turn scenarios in asphalt terrain (a), grass terrain (b), and rough field terrain (c). Red color indicates scenarios with cargo and blue color indicates scenarios without cargo. The robot makes two turns of a 0.5 m radius that last 8 s each. The first occurs in the time interval between 11 and 19 s, and the second in the time interval between 22 and 30 s. As depicted in Figure 11a through Figure 11c, no extreme fluctuations are observed during the period that the robot turns, which is quite difficult to distinguish from the straight-line consumption pattern. Some occasional peaks, especially on rough field terrain with cargo, are more likely to be attributed to surface imperfections than to the turn actions themselves. A small rise in consumption is observed, though, at the beginning of each different action, especially with cargo on rough field terrain, which drops afterwards.
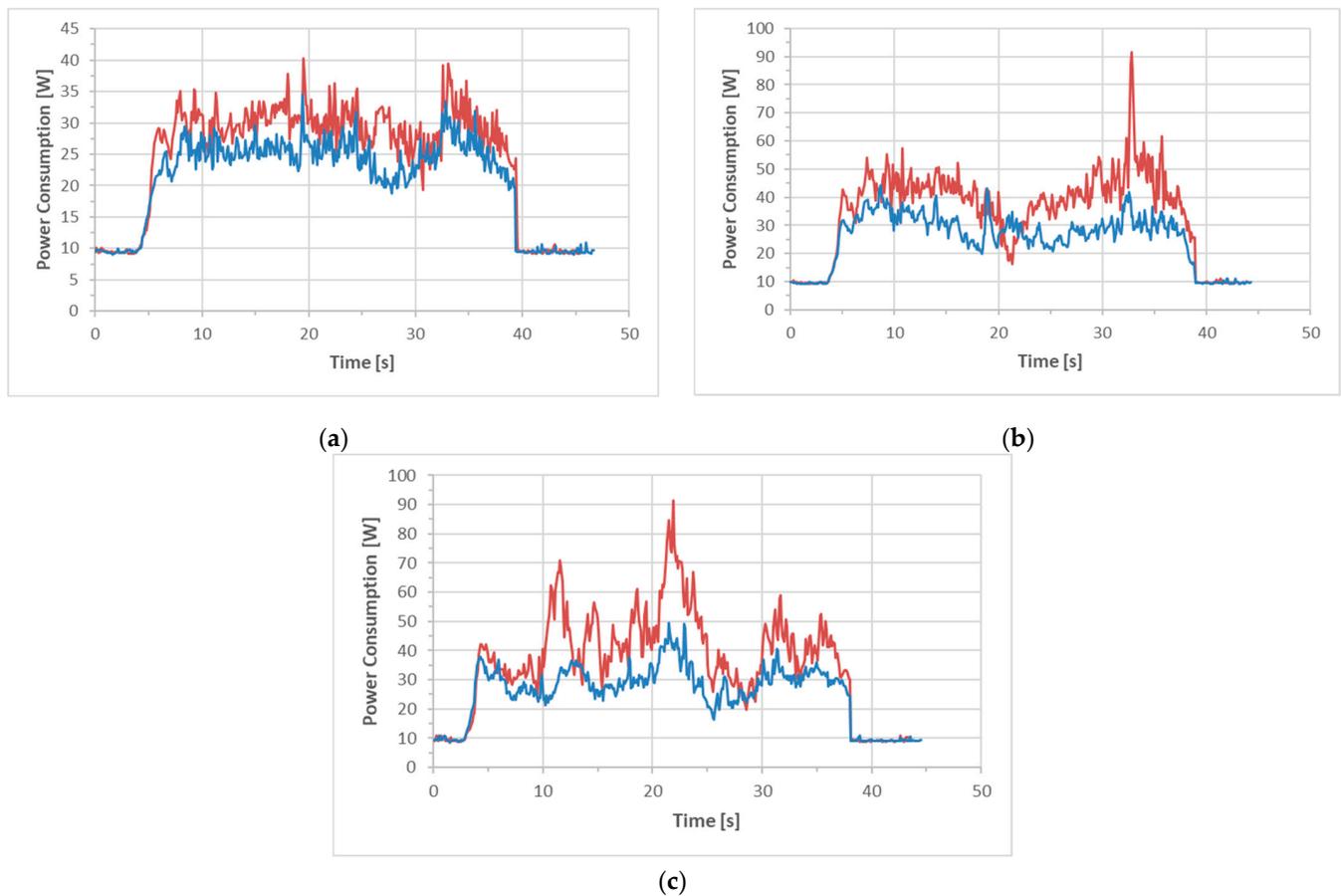

(**a**)   (**b**)

(**c**)

Figure 11. Power consumption with (red color) and without (blue color) cargo for the U-turn scenario on the following: (**a**) asphalt terrain; (**b**) grass terrain; (**c**) rough field terrain.

Figure 12 presents power consumption in 10% inclined asphalt terrain. The robot moves in a straight line with a constant speed in the first scenario (a) at 40% of its maximum speed and, in the second scenario, (b) at 80% of its maximum speed. In Figure 12a, the inclined surface starts at the 60th second and, in Figure 12b, at 35th second, i.e., at the exact moments that a rise in power consumption is observed, it is stabilized to its maximum (i.e., to 10%) between the 95th and 150th second, and between the 55th and 85th second, respectively, and then drops again until horizontal.
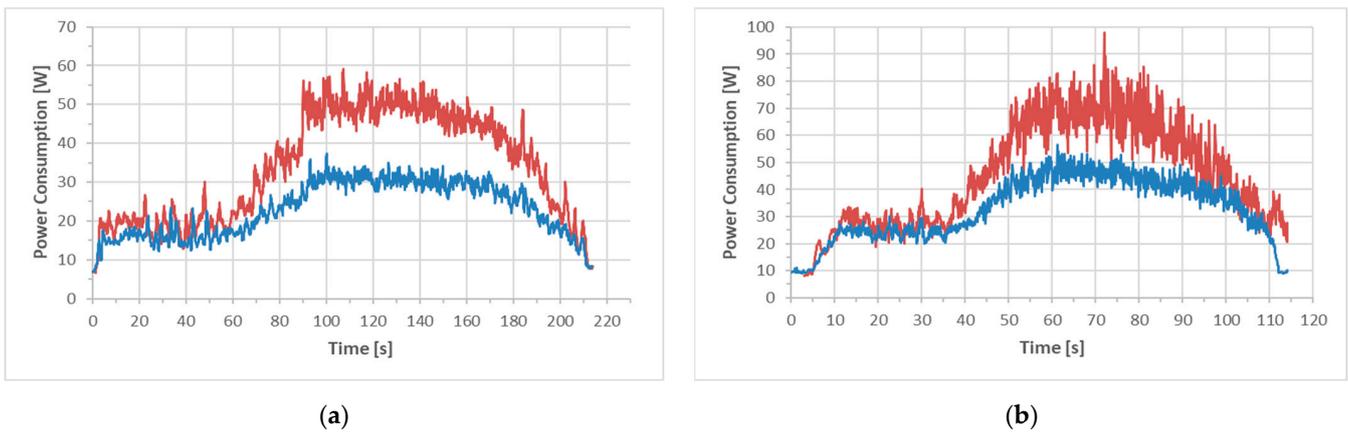
(**a**)

(**b**)

Figure 12. Power consumption during the robot's straight-line motion in 10% inclined asphalt terrain with constant speed: (**a**) 40% of the robot's maximum speed; (**b**) 80% of the robot's maximum speed. Blue color indicates without cargo scenario and red color with cargo scenario.

Figure 13a presents the power consumption of the robotic vehicle with lead–acid (blue color) and Li-Po (red color) batteries in the steps scenario without cargo at 0.3 m/s and at 0.6 m/s on asphalt terrain.
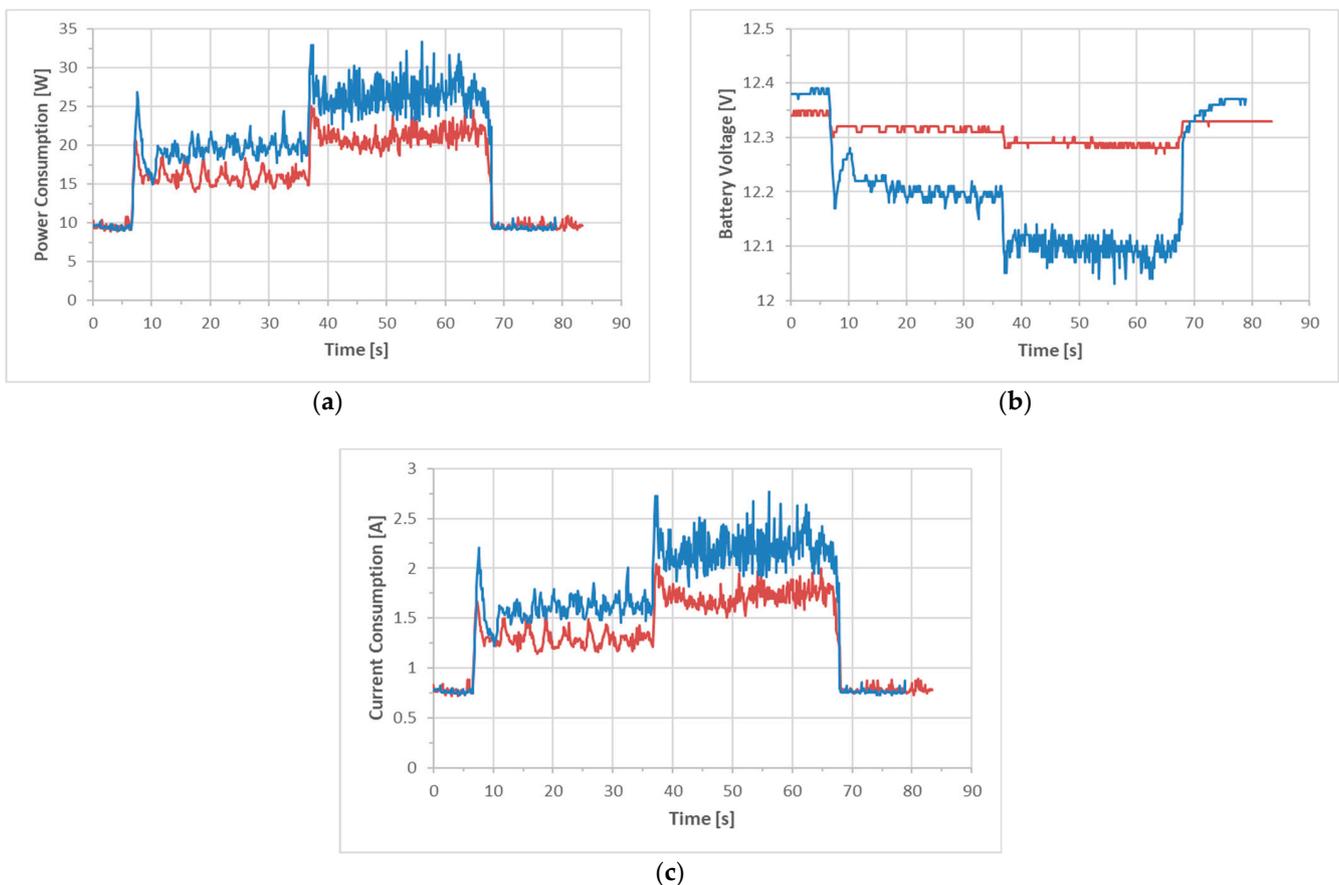

(**a**)

(**b**)

(**c**)

Figure 13. Comparative energy diagrams between sealed lead–acid (blue color) and LiPo (red color) batteries for the steps without cargo scenario in asphalt terrain: (**a**) power consumption in Watt; (**b**) battery voltage in Volt; (**c**) current consumption in Ampere.

As can been seen in Figure 13a and Table 4, Li-Po batteries provide lower power consumption due to their reduced weight and their lower internal resistance. Sealed

lead–acid batteries weigh 2.1 kg each, resulting in a 4.2 kg total battery weight, while Li-Po batteries weigh 0.63 kg each, resulting in a 1.26 kg total weight, merely 30% of the sealed lead–acid batteries' weight. Additionally, Li-Po batteries display less voltage drops, as can been seen in Figure 13b and Table 5 from the voltage deviation calculation. These voltage drops have a significant negative impact on battery life cycle and may cause disturbances in the system's electronics. Figure 13c presents the current consumption for this specific scenario.

Table 4. Power consumption comparison between lead–acid and Li-Po batteries in the steps without cargo in the asphalt terrain scenario.

Steps without Cargo in Asphalt Terrain	P Average at 40% Speed	P Average at 80% Speed
Lead–acid Batteries	19.4 W	26.6 W
Li-Po Batteries	15.9 W	21.2 W

Table 5. Battery voltage comparison between lead–acid and Li-Po batteries in the steps without cargo in the asphalt terrain scenario.

Steps without Cargo in Asphalt Terrain	V Deviation at 40% Speed	V Deviation at 80% Speed
Lead–acid Batteries	0.028	0.019
Li-Po Batteries	0.007	0.006

Figure 14a presents the power consumption of the robotic vehicle with lead–acid and LiPo batteries in the steps without cargo scenario in the grass terrain. The diagram and Table 6 prove that LiPo batteries provide less power consumption because of their reduced weight and their lower internal resistance. In most cases, LiPo batteries exhibit lower voltage sags as well as less power consumption and voltage deviations than the lead–acid ones because of their lower weight and internal resistance, as can be seen in Figure 14b, Table 6, and Table 7, respectively.
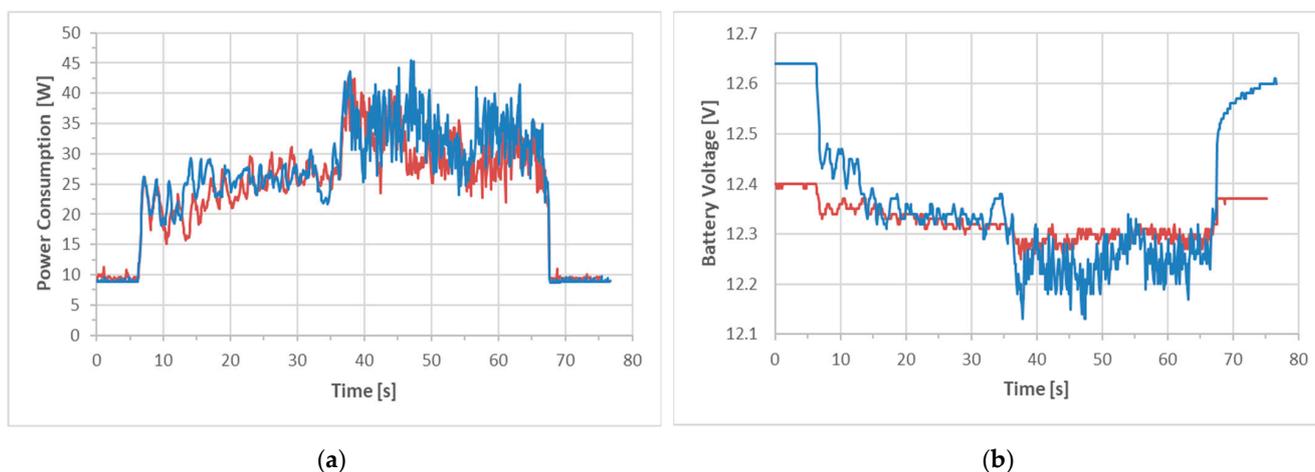

(**a**) (**b**)

Figure 14. Comparative power and voltage variations between lead–acid (blue color) and LiPo (red color) batteries for the steps without cargo scenario in grass terrain: (**a**) power consumption; (**b**) battery voltage.

Table 6. Power consumption comparison between lead–acid and Li-Po batteries in the steps without cargo in the grass terrain scenario.

Steps without Cargo in Grass Terrain	P Average at 40% Speed	P Average at 80% Speed
Lead–acid Batteries	24.8 W	33.7 W
Li-Po Batteries	23.7 W	30.9 W

Table 7. Battery voltage comparison between lead–acid and Li-Po batteries in the steps without cargo in the grass terrain scenario.

Steps without Cargo in Grass Terrain	V Deviation at 40% Speed	V Deviation at 80% Speed
Lead–acid Batteries	0.049	0.041
Li-Po Batteries	0.018	0.014

As can be seen in Figure 15a and Table 8, LiPo batteries provide lower power consumption than lead–acid in the steps with the cargo scenario in the rough field terrain. Typically, LiPo batteries have a flatter voltage discharge curve compared to lead–acid batteries, which means their voltage remains relatively stable, as can be seen in Figure 15b, as well as displaying less power and voltage deviations, as is presented in Tables 8 and 9, respectively. However, at lower speeds (40% of the maximum), the load on the batteries might be relatively light, which could lead to voltage deviations, impacting a lot on the power deviation, as can be seen in Table 8.
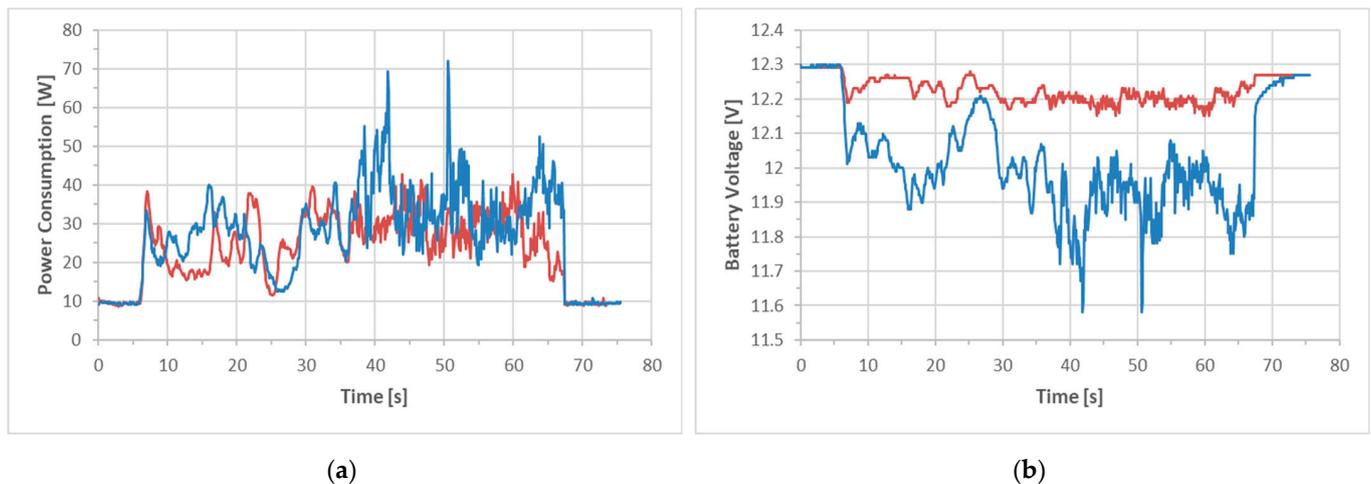

(**a**)   (**b**)

Figure 15. Comparative energy diagrams between lead–acid (blue color) and LiPo (red color) batteries for the steps with cargo scenario in rough field terrain: (**a**) power consumption in Watt; (**b**) battery voltage in Volt.
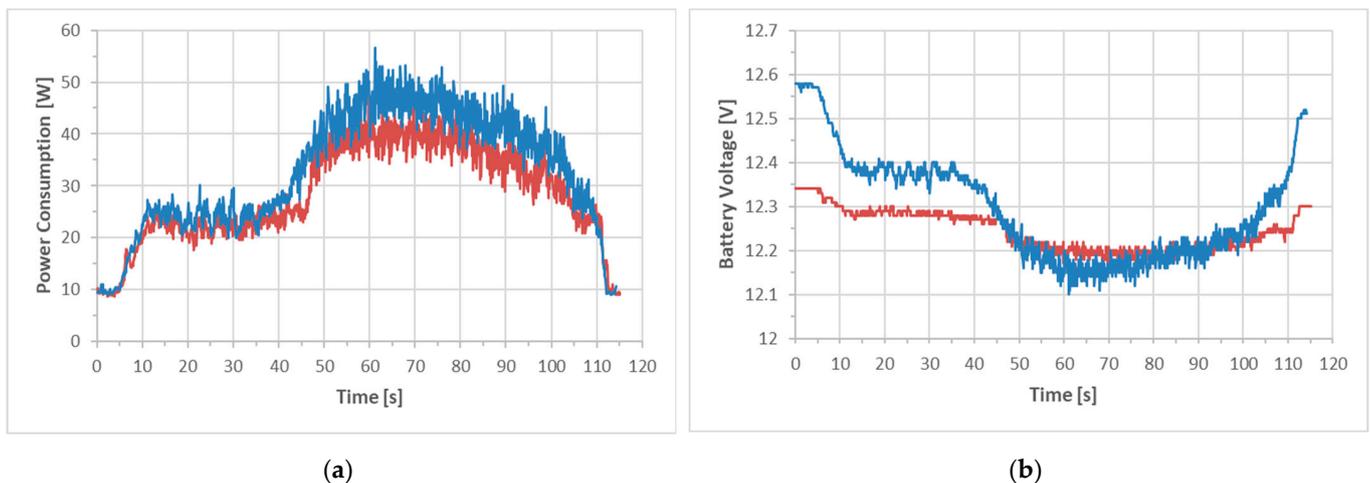
Table 8. Power consumption comparison between lead–acid and Li-Po batteries in the steps with cargo in the rough field terrain scenario.

Steps with Cargo in Rough Field Terrain	P Average at 40% Speed	P Average at 80% Speed
Lead–acid Batteries	25.5 W	35.5 W
Li-Po Batteries	24.6 W	29.0 W

Table 9. Battery voltage comparison between lead–acid and Li-Po batteries in the steps with cargo in the rough field terrain scenario.

Steps with Cargo in Rough Field Terrain	V Deviation at 40% Speed	V Deviation at 80% Speed
Lead–acid Batteries	0.085	0.089
Li-Po Batteries	0.028	0.019

Figure 16a presents the power consumption with lead–acid and LiPo batteries as the robot moves in straight line in a 10% inclined asphalt terrain with 80% of its maximum speed and without cargo. The inclined surface begins at 42 s, where power consumption starts rising and the battery voltage starts dropping. The inclined surface ends at 105 s, where the power consumption and the battery voltage drop again to the flat surface levels. As expected, voltage in LiPo batteries is relatively more stable than in lead–acid ones (Figure 16b) and the LiPo batteries provide less power and less voltage deviation due to their reduced weight and internal resistance, as can be seen in Tables 10 and 11, respectively.

(**a**)   (**b**)

Figure 16. Comparative energy diagrams between lead–acid (blue color) and LiPo (red color) batteries during the robot's straight-line movement in 10% inclined asphalt terrain with 80% of its maximum speed and without cargo: (**a**) power consumption in Watt; (**b**) battery voltage in Volt.

Table 10. Power consumption comparison between lead–acid and Li-Po batteries in the steps with 80% speed without cargo in the inclined asphalt terrain scenario.

Steps with 80% Speed without Cargo in Inclined Asphalt Terrain	P Average
Lead–acid Batteries	35.8 W
Li-Po Batteries	30.5 W

Table 11. Battery voltage comparison between lead–acid and Li-Po batteries in the steps with 80% speed without cargo in inclined asphalt terrain scenario.

Steps with 80% Speed without Cargo in Inclined Asphalt Terrain	V Deviation
Lead–acid Batteries	0.090
Li-Po Batteries	0.040

4. Discussion

In the existing literature, there are numerous studies discussing strategies for developing intelligent vehicles. However, there is a lack of studies focusing on the energy efficiency of electric robot vehicles in the agricultural sector. Therefore, there is a need for

a more comprehensive examination and analysis of the performance of existing robotic vehicle structures that align with contemporary trends, particularly those moving towards electrification, intelligence, and autonomy. In this regard, the work being presented discusses the applicability and the usefulness of a simple and cost-effective mechanism for detailed power consumption logging on a lightweight electric cargo vehicle, and reports on the corresponding footprint capturing performance during a variety of typical operation scenarios. The specific robotic vehicle is a prototype able for either manual or autonomous operation, according to specific directions and scenarios.

Widely available and well-documented components, such as Arduino microcontrollers and Raspberry Pi board computers, along with accurate sensors and smart phone/tablet compatible software, were utilized in the present work, offering a fluent, friendly, and easy-to-modify environment to execute the necessary experiments. This is a satisfactory solution to the problem of many existing robotic vehicles that do not provide detailed performance measurements, such as power and voltage metrics, or which do not offer enough data space for storing them. It is worth noting that almost no additional cost was needed for the deployment of the proposed mechanism, as it utilizes components that already existed on the cargo robot for its autonomous operation. Nevertheless, especially the low-level part of its functionality (i.e., as explained in Figure 2) can be easily replicated by other researchers utilizing cheap independent microcontrollers such as a second Arduino Uno one or a cheaper NodeMCU that offers Wi-Fi connectivity with the main computer (i.e., the Raspberry Pi) unit.

Results indicate that the power consumption of the robot always remains modest, i.e., between 1 and 2 W/kg, even during extreme conditions. The roughness of the terrain has a smaller impact than initially expected on the power draw, while its target speed direction and especially the surface inclination remain the dominant factors increasing the amperage consumption. It is worth noting that the consumption at idling of the robot used in this study, as reflected at the beginning and at the end of the power traces presented in Section 3.2, typically ranging from 8 W to 10 W, was not negligible. This is due to the needs of its control logic, but this consumption is a constant quantity that can be easily anticipated or modeled via processing. Under this assumption, the impact of the cargo load on the power consumption of the robot was in accordance with its gross weight, as expected.

It must be noted that, due to the electromechanical design and the control arrangements being followed (i.e., to lower the speed of the inner driving wheel and to turn properly the tilting wheel according to the geometry of the robot and the sharpness of the turn), the prototype robotic vehicle was keeping its consumption at very reasonable levels during the scenarios including turns. This is an important advantage compared with a typical tracked or skid steering wheeled vehicle. Indeed, the analysis of power consumption vs. steering radius for either tracked or wheeled robots utilizing the common skid steering method indicated a very high consumption (i.e., of four or five times more) during turns of a small radius [61], such as the ones necessary in the agricultural terrains while maneuvering between plant rows, which is translated into elongated periods of high consumption, given the low speed of the agricultural vehicles while maneuvering. On the other hand, the wheeled layout being used offers better energy autonomy and less electromechanical stress for the components comprising the electric cargo vehicle, which typically doubles or triples its net weight while loaded.

In addition, a main drawback of electrically powered robots is their limited operational time due to the restricted storage capacity of electrical energy. This issue is exacerbated in agriculture due to difficulties in accessing charging points, as these robots often operate in areas distant from the local power infrastructure, making the efficiency of the battery crucial. Two of the most prominent battery types are lead–acid and lithium-ion-polymer (Li-Po) ones. Lead–acid batteries have the lowest cost, but, at the same time, they provide the lowest energy density per unit mass due to their higher weight [62]. They are mainly used in situations where cost is essential, and the operating distance and weight are not

so important [63]. On the other hand, Li-Po batteries are the most expensive ones, but they provide higher energy density, higher charging rates, and deeper discharge cycles, making them the most efficient ones in situations requiring high energy demands [53]. The results of the comparison between Li-Po and lead–acid batteries showed that the Li-Po batteries exhibit considerably less voltage fluctuations and lower total power consumption, due to their lighter weight and lower internal resistance, across all testing scenarios. The fluctuations can substantially negatively affect battery cycles and may lead to disruptions in the electronics of a system. Therefore, Li-Po batteries offer higher efficiency and overall performance in comparison to their lead–acid counterparts. The smaller weight and size provided by the Li-Po batteries can be exploited to increase the overall energy capacity of the electric cargo vehicle, and thus its autonomy, by adding more battery units, to easily match or to exceed the working hour profile of a human worker.

This study aimed to enhance the modeling of agricultural robot activities and provide essential guidelines for behavior assessment, particularly concerning power supply requirements. Therefore, the performance evaluation results can be used for creating accurate models for energy profile emulator and simulator implementations [48]. They can also serve as a basis for the successful performance estimation and optimization of autonomous electric robotic vehicles of considerably different size and role, due to the well-defined relation between size and consumption for this type of vehicles [50,55,56]. Apart from this, similar power data traces can be used for activity characterization and for optimal automatic operational setting adjustments if combined with machine-learning techniques in ways like those proposed in [64,65].

5. Conclusions

This work, utilizing a prototype lightweight autonomous electric cargo robot of open hardware and software philosophy, highlighted a simple and cost-effective methodology for accurate power consumption behavior capturing, at a fine time granularity, and analyzed the corresponding energy performance throughout a variety of characteristic activity scenarios. Due to the common tools being used, even non-expert users could conduct the experiments, while directions were provided for the potential use of the data being collected. Given the well-defined connection between the size and the consumption of the electric robotic vehicles, the energy performance evaluation practices and results collected for the agricultural cargo robot participating in the experiments can serve as a flagship case and a basis for further studies in the area, such as energy consumption profile modeling and optimization and energy demand prediction.

References

1. UNDESA. *World Population Prospects 2022: Summary of Results*; United Nations Department of Economic and Social Affairs: New York, NY, USA, 2022; Available online: https://www.un.org/development/desa/pd/sites/www.un.org.development.desa.pd/files/wpp2022_summary_of_results.pdf (accessed on 10 October 2023).
2. FAO. *The State of the World's Land and Water Resources for Food and Agriculture: Managing Systems at Risk*; FAO: Rome, Italy, 2018.
3. O'Grady, M.J.; O'Hare, G.M. Modelling the smart farm. *Inf. Process. Agric.* **2017**, *4*, 179–187. [CrossRef]
4. Beloev, I.; Kinaneva, D.; Georgiev, G.; Hristov, G.; Zahariev, P. Artificial Intelligence-Driven Autonomous Robot for Precision Agriculture. *Acta Technol. Agric.* **2021**, *24*, 48–54. [CrossRef]
5. Bechar, A.; Vigneault, C. Agricultural robots for field operations: Concepts and components. *Biosyst. Eng.* **2016**, *149*, 94–111. [CrossRef]

6. Bechar, A.; Vigneault, C. Agricultural robots for field operations. Part 2: Operations and systems. *Biosyst. Eng.* **2017**, *153*, 110–128. [CrossRef]

7. Krishna, K.R. *Push Button Agriculture: Robotics, Drones, Satellite-Guided Soil and Crop Management*; Apple Academic Press: Oakville, ON, Canada, 2016; ISBN 978-1-77188-305-4.

8. Bochtis, D.; Benos, L.; Lampridi, M.; Marinoudi, V.; Pearson, S.; Sørensen, C.G. Agricultural Workforce Crisis in Light of the COVID-19 Pandemic. *Sustainability* **2020**, *12*, 8212. [CrossRef]

9. Ridley, W.; Devadoss, S. The Effects of COVID-19 on Fruit and Vegetable Production. *Appl. Econ. Perspect. Policy* **2021**, *43*, 329–340. [CrossRef] [PubMed]

10. Carolan, M. Automated agrifood futures: Robotics, labor and the distributive politics of digital agriculture. *J. Peasant. Stud.* **2020**, *47*, 184–207. [CrossRef]

11. Pessina, D.; Facchinetti, D. A survey on fatal accidents for overturning of agricultural tractors in Italy. *Chem. Eng. Trans.* **2017**, *58*, 79–84. [CrossRef]

12. Botta, A.; Cavallone, P.; Baglieri, L.; Colucci, G.; Tagliavini, L.; Quaglia, G. A Review of Robots, Perception, and Tasks in Precision Agriculture. *Appl. Mech.* **2022**, *3*, 830–854. [CrossRef]

13. Lamborelle, A.; Álvarez, L.F. Farming 4.0: The Future of Agriculture? Available online: https://www.euractiv.com/section/agriculture-food/infographic/farming-4-0-the-future-of-agriculture/ (accessed on 20 October 2023).

14. King, A. Technology: The Future of Agriculture. *Nat. Cell Biol.* **2017**, *544*, S21–S23. [CrossRef] [PubMed]

15. Shamshiri, R.R.; Weltzien, C.; Hameed, I.A.; Yule, I.J.; Grift, T.E.; Balasundram, S.K.; Pitonakova, L.; Ahmad, D.; Chowdhary, G. Research and development in agricultural robotics: A perspective of digital farming. *Int. J. Agric. Biol. Eng.* **2018**, *11*, 1–14. [CrossRef]

16. Fountas, S.; Gemtos, T.A.; Blackmore, S. Robotics and Sustainability in Soil Engineering. In *Soil Engineering*; Springer: Berlin, Germany, 2010; pp. 69–80.

17. Tazzari, R.; Mengoli, D.; Marconi, L. Design Concept and Modelling of a Tracked UGV for Orchard Precision Agriculture. In Proceedings of the 2020 IEEE International Workshop on Metrology for Agriculture and Forestry (MetroAgriFor), Trento, Italy, 4–6 November 2020; pp. 207–212. [CrossRef]

18. Loukatos, D.; Petrongonas, E.; Manes, K.; Kyrtopoulos, I.-V.; Dimou, V.; Arvanitis, K.G. A Synergy of Innovative Technologies towards Implementing an Autonomous DIY Electric Vehicle for Harvester-Assisting Purposes. *Machines* **2021**, *9*, 82. [CrossRef]

19. Habib, A.K.M.R.R.; Butler, K. Environmental and economic comparison of hydrogen fuel cell and battery electric vehicles. *Future Technol.* **2022**, *1*, 25–33. [CrossRef]

20. Khalid, R.; Conjobeeharry, V.; Sanai, A.S.; Brown, C.H.T.; Afrouzi, H.N.; Hassan, A. The feasibility and analysis of electric taxi vehicles in Singapore: A review. *Future Energy* **2023**, *2*, 38–48. [CrossRef]

21. Habib, A.K.M.R.R.; Butler, K. Alternatives to lithium-ion batteries in electric vehicles. *Future Technol.* **2022**, *1*, 33–34. [CrossRef]

22. Teixeira, H.M.; Van den Berg, L.; Cardoso, I.M.; Vermue, A.J.; Bianchi, F.J.J.A.; Peña-Claros, M.; Tittonell, P. Understanding Farm Diversity to Promote Agroecological Transitions. *Sustainability* **2018**, *10*, 4337. [CrossRef]

23. Gorjian, S.; Ebadi, H.; Trommsdorff, M.; Sharon, H.; Demant, M.; Schindele, S. The advent of modern solar-powered electric agricultural machinery: A solution for sustainable farm operations. *J. Clean. Prod.* **2021**, *292*, 126030. [CrossRef]

24. Gorjian, S.; Minaei, S.; MalehMirchegini, L.; Trommsdorff, M.; Shamshiri, R.R. Applications of solar PV systems in agricultural automation and robotics. In *Photovoltaic Solar Energy Conversion*; Elsevier: Amsterdam, The Netherlands, 2020; Chapter 7; pp. 191–235.

25. Klokov, A.V.; Loktionov, E.Y.; Loktionov, Y.V.; Panchenko, V.A.; Sharaborova, E.S. A Mini-Review of Current Activities and Future Trends in Agrivoltaics. *Energies* **2023**, *16*, 3009. [CrossRef]

26. Pearson, S.; Camacho-Villa, T.C.; Valluru, R.; Gaju, O.; Rai, M.C.; Gould, I.; Brewer, S.; Sklar, E. Robotics and Autonomous Systems for Net Zero Agriculture. *Curr. Robot. Rep.* **2022**, *3*, 57–64. [CrossRef]

27. Fountas, S.; Mylonas, N.; Malounas, I.; Rodias, E.; Hellmann Santos, C.; Pekkeriet, E. Agricultural Robotics for Field Operations. *Sensors* **2020**, *20*, 2672. [CrossRef] [PubMed]

28. Lowenberg-DeBoer, J.; Huang, I.Y.; Grigoriadis, V.; Blackmore, S. Economics of robots and automation in field crop production. *Precis. Agric.* **2020**, *21*, 278–299. [CrossRef]

29. Marinoudi, V.; Sørensen, C.G.; Pearson, S.; Bochtis, D. Robotics and labour in agriculture. A context consideration. *Biosyst. Eng.* **2019**, *184*, 111–121. [CrossRef]

30. World Health Organization (WHO). Disability. 2023. Available online: https://www.who.int/disabilities/en/ (accessed on 5 November 2023).

31. Grimstad, L.; From, P.J. The Thorvald II agricultural robotic system. *Robotics* **2017**, *6*, 24. [CrossRef]

32. Saga Robotics. The Official Site of Saga Robotics. 2021. Available online: https://sagarobotics.com/ (accessed on 10 October 2023).

33. Rangarajan, S.S.; Sunddararaj, S.P.; Sudhakar, A.; Shiva, C.K.; Subramaniam, U.; Collins, E.R.; Senjyu, T. Lithium-Ion Batteries—The Crux of Electric Vehicles with Opportunities and Challenges. *Clean Technol.* **2022**, *4*, 908–930. [CrossRef]

34. Razmjoo, A.; Ghazanfari, A.; Jahangiri, M.; Franklin, E.; Denai, M.; Marzband, M.; Astiaso Garcia, D.; Maheri, A. A Comprehensive Study on the Expansion of Electric Vehicles in Europe. *Appl. Sci.* **2022**, *12*, 11656. [CrossRef]

35. Gonzalez-de-Santos, P.; Fernández, R.; Sepúlveda, D.; Navas, E.; Emmi, L.; Armada, M. Field Robots for Intelligent Farms—Inhering Features from Industry. *Agronomy* **2020**, *10*, 1638. [CrossRef]

36. Harrop, P.; Dent, M. Electric Vehicles and Robotics in Agriculture 2020–2030, IDTechEx. Available online: https://www.idtechex.com/en/research-report/electric-vehicles-and-robotics-in-agriculture-2020-2030/717 (accessed on 20 October 2023).

37. Onishi, Y.; Yoshida, T.; Kurita, H.; Fukao, T.; Arihara, H.; Iwai, A. An automated fruit harvesting robot by using deep learning. *Robomech J.* **2019**, *6*, 13. [CrossRef]

38. Etienne, A.; Saraswat, D. Machine learning approaches to automate weed detection by UAV based sensors. In Proceedings of the Autonomous Air and Ground Sensing Systems for Agricultural Optimization and Phenotyping IV, Baltimore, MD, USA, 15–16 April 2019; Volume 11008, pp. 202–215.

39. Abioye, E.A.; Hensel, O.; Esau, T.J.; Elijah, O.; Abidin, M.S.Z.; Ayobami, A.S.; Nasirahmadi, A. Precision irrigation management using machine learning and digital farming solutions. *AgriEngineering* **2022**, *4*, 70–103. [CrossRef]

40. Zhang, G.; Li, G.; Peng, J. Risk Assessment and Monitoring of Green Logistics for Fresh Produce Based on a Support Vector Machine. *Sustainability* **2020**, *12*, 7569. [CrossRef]

41. Fei, Z.; Vougioukas, S.G. Co-robotic harvest-aid platforms: Real-time control of picker lift heights to maximize harvesting efficiency. *Comput. Electron. Agric.* **2021**, *180*, 105894. [CrossRef]

42. Peng, C.; Vougioukas, S.; Slaughter, D.; Fei, Z.; Arikapudi, R. A strawberry harvest-aiding system with crop-transport collaborative robots: Design, development, and field evaluation. *J. Field Robot.* **2022**, *39*, 1231–1257. [CrossRef]

43. Yépez-Ponce, D.F.; Salcedo, J.V.; Rosero-Montalvo, P.D.; Sanchis, J. Mobile robotics in smart farming: Current trends and applications. *Front. Artif. Intell.* **2023**, *6*, 1213330. [CrossRef]

44. Ferreira, J.F.; Portugal, D.; Andrada, M.E.; Machado, P.; Rocha, R.P.; Peixoto, P. Sensing and Artificial Perception for Robots in Precision Forestry: A Survey. *Robotics* **2023**, *12*, 139. [CrossRef]

45. Oliveira, L.F.P.; Moreira, A.P.; Silva, M.F. Advances in Agriculture Robotics: A State-of-the-Art Review and Challenges Ahead. *Robotics* **2021**, *10*, 52. [CrossRef]

46. Mantoam, E.J.; Romanelli, T.L.; Gimenez, L.M. Energy demand and greenhouse gases emissions in the life cycle of tractors. *Biosyst. Eng.* **2016**, *151*, 158–170. [CrossRef]

47. Tassielli, G.; Renzulli, P.A.; Mousavi-Avval, S.H.; Notarnicola, B. Quantifying life cycle inventories of agricultural field operations by considering different operational parameters. *Int. J. Life Cycle Assess.* **2019**, *24*, 1075–1092. [CrossRef]

48. Lampridi, M.; Kateris, D.; Sørensen, C.G.; Bochtis, D. Energy Footprint of Mechanized Agricultural Operations. *Energies* **2020**, *13*, 769. [CrossRef]

49. Zhang, J.; Wang, Z.; Liu, P.; Zhang, Z. Energy consumption analysis and prediction of electric vehicles based on real-world driving data. *Appl. Energy* **2020**, *275*, 115408. [CrossRef]

50. Weiss, M.; Cloos, K.C.; Helmers, E. Energy efficiency trade-offs in small to large electric vehicles. *Environ. Sci. Eur.* **2020**, *32*, 46. [CrossRef]

51. Ma, J.; Zhu, Y.; Chen, D.; Zhang, C.; Song, M.; Zhang, H.; Chen, J.; Zhang, K. Analysis of Urban Electric Vehicle Adoption Based on Operating Costs in Urban Transportation Network. *Systems* **2023**, *11*, 149. [CrossRef]

52. Rimpas, D.; Kaminaris, S.D.; Piromalis, D.D.; Vokas, G.; Arvanitis, K.G.; Karavas, C.-S. Comparative Review of Motor Technologies for Electric Vehicles Powered by a Hybrid Energy Storage System Based on Multi-Criteria Analysis. *Energies* **2023**, *16*, 2555. [CrossRef]

53. Mikołajczyk, T.; Mikołajewski, D.; Kłodowski, A.; Łukaszewicz, A.; Mikołajewska, E.; Paczkowski, T.; Macko, M.; Skornia, M. Energy Sources of Mobile Robot Power Systems: A Systematic Review and Comparison of Efficiency. *Appl. Sci.* **2023**, *13*, 7547. [CrossRef]

54. Loukatos, D.; Templalexis, C.; Lentzou, D.; Xanthopoulos, G.; Arvanitis, K.G. Enhancing a flexible robotic spraying platform for distant plant inspection via High-Quality thermal imagery data. *Comput. Electron. Agric.* **2021**, *190*, 106462. [CrossRef]

55. Chang, N.; Baek, D.; Hong, J. Power Consumption Characterization, Modeling and Estimation of Electric Vehicles. In Proceedings of the 2014 IEEE/ACM International Conference on Computer-Aided Design (ICCAD), San Jose, CA, USA, 2–6 November 2014. [CrossRef]

56. Jung, H.; Silva, R.; Han, M. Scaling Trends of Electric Vehicle Performance: Driving Range, Fuel Economy, Peak Power Output, and Temperature Effect. *World Electr. Veh. J.* **2018**, *9*, 46. [CrossRef]

57. Gravity. The Gravity I2C Digital Wattmeter Module Using the INA219 Chip. Available online: https://www.dfrobot.com/product-1827.html (accessed on 20 October 2023).

58. ZED-F9P. The SparkFun ZED-F9P GPS-RTK2 Board Description. Available online: https://www.sparkfun.com/products/15136 (accessed on 20 October 2023).

59. App Inventor. The MIT App Inventor Programming Environment. 2023. Available online: http://appinventor.mit.edu/explore/ (accessed on 20 September 2023).

60. QGIS. A Free and Open Source Geographic Information System. 2023. Available online: https://www.qgis.org/en/site/ (accessed on 20 September 2023).

61. Guo, T.; Guo, J.; Huang, B.; Peng, H. Power consumption of tracked and wheeled small mobile robots on deformable terrains–model and experimental validation. *Mech. Mach. Theory* **2019**, *133*, 347–364. [CrossRef]

62. May, G.J.; Davidson, A.; Monahov, B. Lead batteries for utility energy storage: A review. *Energy Storage* **2018**, *15*, 145–157. [CrossRef]

63. Budde-Meiwes, H.; Drillkens, J.; Lunz, B.; Muennix, J.; Rothgang, S.; Kowal, J.; Sauer, D.U. A review of current automotive battery technology and future prospects. *Proc. Inst. Mech. Eng. Part D J. Automob. Eng.* **2013**, *227*, 761–776. [CrossRef]

64. Petruschke, L.; Walther, J.; Burkhardt, M.; Luther, M.; Weigold, M. Machine learning based identification of energy states of metal cutting machine tools using load profiles. *Procedia CIRP* **2021**, *104*, 357–362. [CrossRef]

65. Tan, D.; Suvarna, M.; Tan, Y.S.; Li, J.; Wang, X. A three-step machine learning framework for energy profiling, activity state prediction and production estimation in smart process manufacturing. *Appl. Energy* **2021**, *291*, 116808. [CrossRef]